## ARTICLE

Check for updates

# Formation of the Xigaze Metamorphic Sole under Tibetan continental lithosphere reveals generic characteristics of subduction initiation

Carl Guilmette [1✉], Douwe J. J. van Hinsbergen[2], Matthijs A. Smit[3], Antoine Godet[4], François Fournier-Roy[1], Jared P. Butler[4], Marco Maffione[5], Shun Li[6] & Kip Hodges[7]

Metamorphic soles found under allochthonous oceanic lithosphere, or ophiolites, are interpreted as derived from lower plate oceanic crust material accreted to upper plate mantle during intraoceanic subduction initiation. Their metamorphic evolution is inferred to reflect the thermal structure at the site of subduction nucleation, with granulite-bearing soles linked to initiation at hot spreading centers. Here we present garnet Lu-Hf geochronology for the granulite-bearing sole of the Xigaze ophiolite in South Tibet, whose oceanic crust formed ~130 Ma through continental forearc extension. Our study shows that sole metamorphism was ongoing by 144 Ma, implying that north-directed subduction began at least 14 million years before oceanic forearc spreading. The upper plate at the time of subduction initiation was thus continental, not oceanic. Our results demonstrate that metamorphic characteristics of soles are independent of the specific tectonic setting at the subduction nucleation site and rather provide generic constraints on the subduction initiation process.

[1] Département de Géologie et de Génie Géologique, Université Laval, Québec, QC, Canada. [2] Department of Earth Sciences, Utrecht University, Utrecht, Netherlands. [3] Department of Earth, Ocean and Atmospheric Sciences, University of British Columbia, Vancouver, BC, Canada. [4] Natural Resources Canada, Geological Survey of Canada, Ottawa, Canada. [5] School of Geography Earth and Environmental Sciences, University of Birmingham, Birmingham, UK. [6] School of Oceanography, Shanghai Jiao Tong University, Shanghai, China. [7] School of Earth and Space Exploration, Arizona State University, Tempe, AZ, USA. ✉email: carl.guilmette@ggl.ulaval.ca

The formation of new subduction zones, or Subduction Initiation (SI), is fundamental to the onset and stabilization of plate tectonics[1], yet the processes and settings involved in the nucleation of a new convergent plate boundary remain challenging to reconstruct[2]. Critical to our understanding of SI are geological records of the incipient subduction plate contact, but these are inaccessible in modern subduction zones. Exposed relics of such interfaces have been recognized in the form of sub-ophiolitic metamorphic soles (soles) – thin slabs of metamorphic rocks found at the base of supra-subduction zone ophiolites and showing an inverted metamorphic gradient[3–6]. These metamorphic rocks are derived from upper oceanic crust and are interpreted as being accreted from the lower to the upper plate during SI[5,7–9]. The overlying supra-subduction zone ophiolites are interpreted as allochthonous relic forearc oceanic lithosphere of the upper plate formed during or shortly after SI[10,11]. Accordingly, the ophiolite-sole association is generally seen as diagnostic of intra-oceanic SI[12,13]. The high-temperature granulite facies peak metamorphic conditions reported in most soles (11–15 kbar, ≥800 °C[7]) are further interpreted as reflecting a high geothermal gradient at the site of SI, leading to the association of ophiolite-sole couples with SI at or near oceanic spreading centers[3,12–14]. However, the inference that ophiolite-sole couples are diagnostic of intra-oceanic SI may be challenged, especially where it can be demonstrated that SI was induced, whereby upper plate extension and ophiolitic crust generation post-dates initial underthrusting[1,15].

Recent studies using garnet Lu-Hf geochronology of garnet-clinopyroxene amphibolite in soles revealed that initial underthrusting may predate upper plate extension and formation of the overlying supra-subduction zone ophiolitic crust by more than 8 Ma[15–17]. Determining the setting of SI therefore requires reconstructing the upper plate lithosphere at the time of metamorphic sole burial, rather than at the time of ophiolitic crust generation[18,19]. This is of particular importance in the case of ophiolite-sole pairs that formed next to continental margins, like the Xigaze Ophiolite[20] and its sole[21,22] in South Tibet.

The Xigaze Ophiolite was generated at the southern margin of the continental Lhasa Terrane of southern Tibet[23,24] through forearc extension[25–27] that generated a slow[28] to ultra-slow[29] spreading center above the north-directed subduction zone that eventually led to the India-Asia collision[30]. Estimates of timing of this SI vary: on the one hand, those using the age of ophiolite spreading and hyperextension as a proxy for the birth of the subduction zone place SI around ~130 Ma, in which case sole formation occurred below the forearc when ophiolites were spreading[21,31,32]. If, on the other hand, ophiolite spreading post-dates SI, then sole formation may have started below the lithosphere within which the ophiolites formed. Such an older SI age of even 170 Ma has been proposed to explain magmatism on the southern Lhasa Terrane[30,33], although this magmatism may also be related to southward subduction along the northern Lhasa margin[34–36]. The current state of the art thus allows for multiple interpretations of SI timing, hampering interpreting the tectonic setting and conditions under which the Xigaze sole formed.

In this paper, we aim to determine the timing of initial lower plate underthrusting through Lu-Hf garnet geochronology, as a direct way to date whether the Xigaze Ophiolite metamorphic sole formed prior to or after forearc extension and ophiolite formation. We therefore investigate garnet-clinopyroxene amphibolite from the Xigaze sole and complement the Lu-Hf garnet isochron ages with Lu trace element maps to support age data interpretation. We discuss the implications of our results for the timing and setting of north-directed SI under the Lhasa margin and for the generic mechanism and setting of sole formation during SI in general.

## Results

**Geological setting and sampling.** The 2000 km long Indus Yarlung Zangbo Suture Zone, in South Tibet (Fig. 1A), exposes the remnants of the Neo-Tethys Ocean that once separated India from the Lhasa Terrane[20]. The central segment hosts the Xigaze Ophiolite (XO), which comprises several ophiolitic massifs (Fig. 1B) that are typically composed, from the base up, of a mantle tectonite section, rare cumulates and gabbro of the lower plutonic crust, a sill/dike complex and pillowed basalts[20,37], and a Lower Cretaceous radiolarian chert[38] sedimentary cover interfingered with arc-derived volcanic ash layers and Lhasa Terrane-derived turbiditic sandstones[23,24]. These Lower Cretaceous ages of the oldest sedimentary cover of the ophiolite are coincident with a ~130 Ma U/Pb zircon age of gabbro of the XO[39], and with similar 130–120 Ma ages along-strike[20,31]. Paleomagnetic data and provenance of the XO sedimentary cover indicate formation at the immediate southern margin of the Lhasa Terrane as a forearc to the Gangdese arc[23,24,26]. The mantle section of the XO has a long history of interaction with subduction fluids and is not genetically related to the overlying crust[40,41]: instead, its characteristics are consistent with at least partial derivation of the XO mantle section from Lhasa Terrane subcontinental lithosphere[25,26,42]. To the South, the ophiolite is overthrusting a sheared serpentinite mélange that contains a dismembered sole[21,22,43] and oceanic lithosphere-derived blocks[44,45]. Farther below is the Bainang subduction complex, a thrust-stack of trench-fill and abyssal radiolarian mudstone and chert offscraped from the Neo-Tethys seafloor during north-directed subduction[46]. This package was eventually thrust onto the continental margin-derived Tethyan Himalayan Sequence in Paleogene time[47].

The XO sole consists of blocks of grt-cpx amphibolites, common amphibolite, and greenschist embedded in the serpentinite matrix of the ophiolitic mélange. The high-pressure granulite blocks show evidence of partial melting as mostly concordant leucosomes[48]. The maximum metamorphic conditions recorded in the grt-cpx amphibolite of the XO sole are in the high-pressure granulite facies ~14 kbar and over 850 °C[22,32,43,48], in agreement with the reported leucosomes, and are consistent with the other soles worldwide[7]. They returned 133–119 Ma U-Pb zircon dates that are interpreted either as post-peak metamorphism or igneous protolith ages[32,48], apatite U-Pb ages of 132–133 Ma[48], and $^{40}Ar/^{39}Ar$ hornblende cooling ages of 130–119 Ma[21,43], all overlapping with the age of overlying ophiolitic crust[39,49]. Such a dismembered sole sharing the same geochronological and petrological characteristics has also been described under the Saga ophiolite, farther west along the central segment of the Yarlung Zangbo Suture Zone[43].

We analyzed four grt-cpx amphibolite specimens in this study, which were sampled from decametric blocks in the ophiolitic mélange of the valley east of Bainang (Fig. 1C, D). Field relationships, petrography, mineral chemistry, geochemistry, and Ar geochronology of these rocks were reported previously[21,22]. All four samples show a hornblende-dominated nematoblastic fabric with anhedral prehnitized plagioclase and slightly coarser-grained grt–cpx-rich horizons (Fig. 2A–D). Both domains show fine-grained ilmenite–titanite symplectites. Garnet of mostly almandine and grossular composition occurs as subhedral centimeter-scale pre- to syn-kinematic porphyroblasts with inclusions of clinopyroxene, plagioclase, hornblende, and titanite/rutile/ilmenite.

**Garnet chemistry.** Garnet grains show remarkably diverse Lu zoning patterns between and within samples (Fig. 2E–H). Garnet from BAI01 exhibits a bell-shaped concentric zoning consistent with Rayleigh fractionation, with Lu content decreasing from core (~10 ppm) to rim (~3 ppm). Garnet from CG64 shows complex
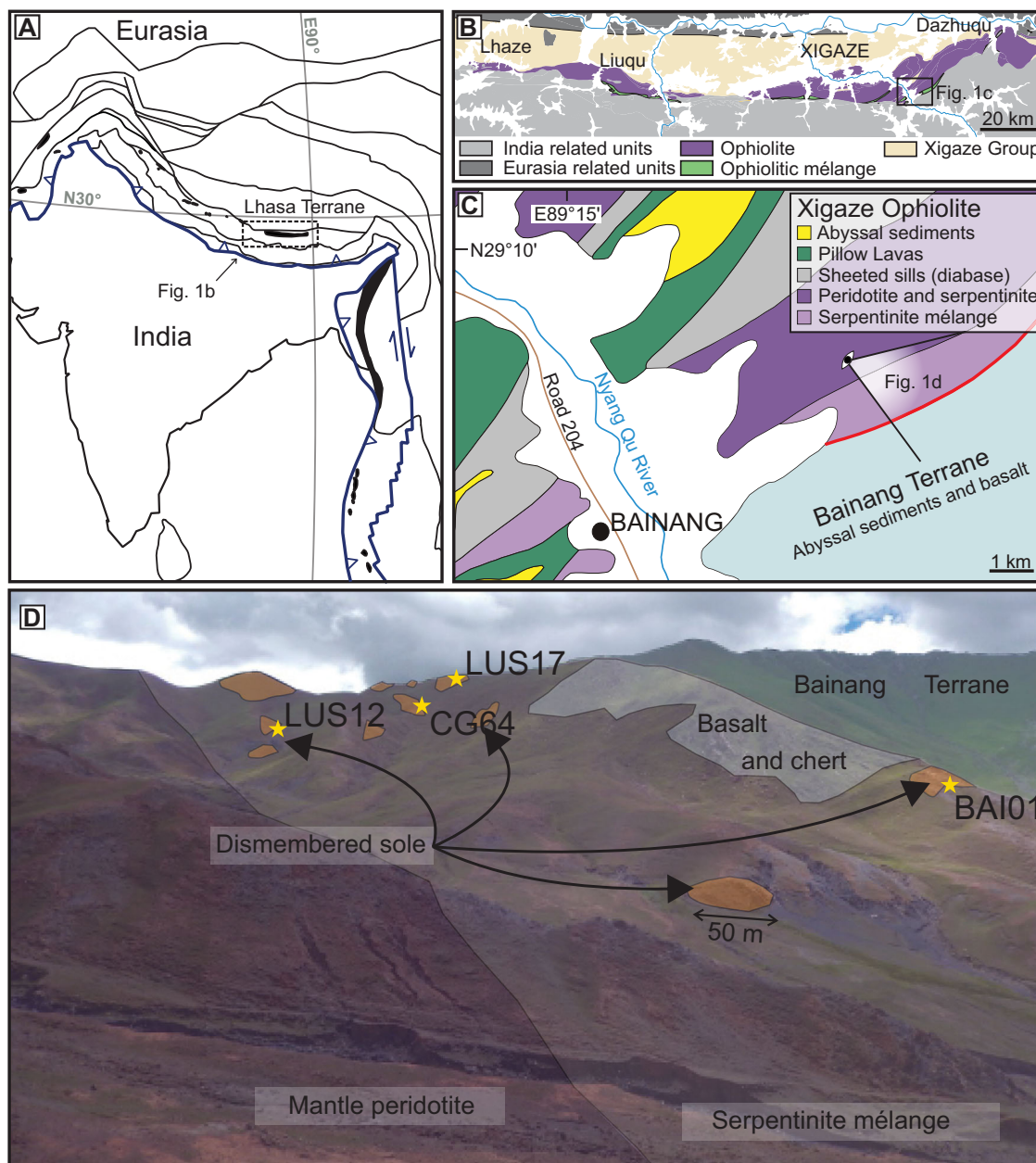
**Fig. 1 Geology of the Xigaze ophiolite and its metamorphic sole. A** Simplified tectonic map of the India-Asia collision zone with major faults and boundaries showing main ophiolite belts (in black) and study area (box B). **B** Simplified geological map of the central segment of the Yarlung Zangbo Suture Zone[77]; location of **C** is indicated. **C** Detailed geological map of the sampling area[77]. Red line is a major south-dipping thrust sense fault; location of **D** is indicated. **D** Field photo of sampling site with geological interpretation and sample location.

zoning with a patchy Lu-depleted core with inherited fabric, a slightly Lu-richer mantle (~6 ppm), and a variably Lu-poor rim (3–4 ppm). Garnet from LUS17 broadly shows homogeneous content, hinting to potential peak diffusion, with clear signs of resorption at some boundaries and associated Lu enrichment (up to 5 ppm). Some sub-grains still retain Rayleigh-type growth zoning (lower left corner of Fig. 2G). Garnet from LUS12 features sharp oscillatory zoning in a generally Lu-poor mantle overgrowing a patchy xenomorphic Lu-richer core (up to 20 ppm).

**Lu-Hf garnet geochronology**. The analyzed samples provided four Lu-Hf garnet ages that were identical within uncertainty (Table 1). Garnet from sample BAI01 yielded a Lu-Hf whole rock-garnet isochron age (Fig. 2I) of $143.7 \pm 0.7$ Ma (MWSD = 1.6; number of garnet analyses $n_{grt} = 4$), whereas that of sample

CG64 (Fig. 2J) yielded a $144.6 \pm 0.9$ Ma isochron (MSWD = 0.52; $n_{grt} = 4$). Garnet fractions were extremely difficult to extract for sample LUS17, mainly due to the fragile nature of grains. The sample yielded an Lu-Hf isochron age (Fig. 2K) of $140.1 \pm 4.5$ Ma (MSWD = 0.12; $n_{grt} = 2$). Garnet from sample LUS12 (Fig. 2L) yielded a $144.3 \pm 3.5$ Ma (MSWD = 0.29; $n_{grt} = 3$) and required omission of the fourth garnet fraction for which the isotopic ratio did not correspond to that of the other fractions. The weighted mean of these four isochron ages is $144.0 \pm 1.2$ Ma (MSWD = 1.8).

## Discussion

**Evolution of the south tibetan metamorphic sole**. The robustness of the Lu–Hf geochronometer[50,51] is largely governed by the diffusivity of Hf, which is demonstrably sluggish[52]. The peak
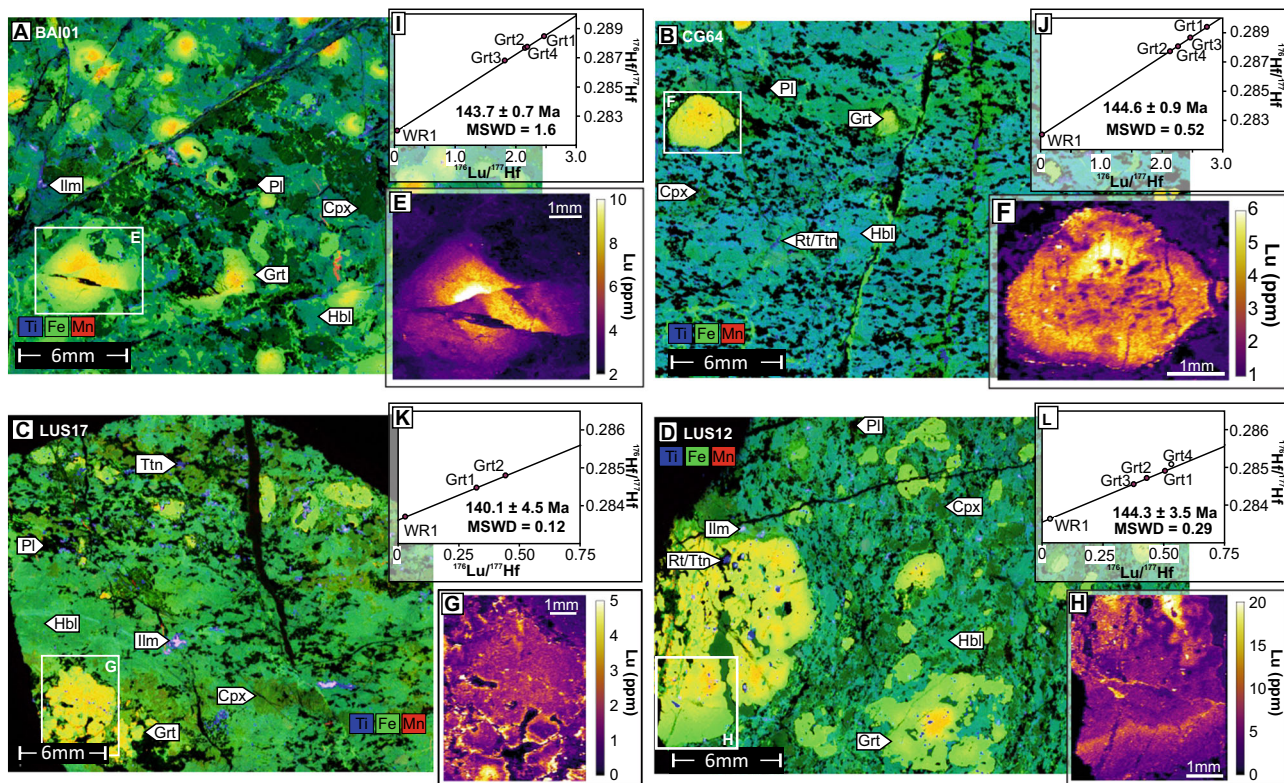
**Fig. 2 Garnet petrochronology. A–D** μ-XRF element scans of thin sections for Fe, Ti and Mn. Pl plagioclase, Hbl hornblende, Ilm ilmenite, Ttn titanite, Ru rutile. **E–H** Lutetium distribution maps of garnet porphyroblasts. **I–L** Lu-Hf garnet isochrons.

temperatures that the Tibetan sole samples were subjected to do not exceed estimated closure temperatures of diffusive Hf loss, which is in excess of 950 °C for grains analyzed in this study[50]. Lutetium is more mobile, so the hypothesized effects of any diffusive net transfer of Lu between garnet and matrix[52] are to be considered. The Lu element maps provide a useful means to do so. The Lu distribution and zoning in garnet from all four samples is different (Fig. 2E–H), both in terms of primary zoning and the degree to which resorption and possible Lu reuptake has affected grains. Yet, despite these differences, the Lu–Hf dates obtained for all samples are identical within uncertainty. The only apparently different age component present among the samples is observed for coarse fragments derived from particularly large grains in LUS12a; this material (fraction Grt4) appears older than most of the garnet in that sample, which is inconsistent with any age bias by Lu redistribution in mafic rocks[52] and instead may indicate inherited cores (Fig. 2H). Regardless, the prevalence of c. 144-Ma Lu-Hf ages for garnet of different average grain size, composition and zoning indicates that actual age bias, either due to differences in zoning or possible diffusive Lu reuptake (e.g., LUS17), did not significantly influence the age data; the Lu-Hf age data thus reliably represents the timing of garnet growth at ~144 Ma. As prograde garnet growth in supracrustal mafic protoliths requires an increase in both P and T, we interpret those growth ages as a minimum age for formation of the XO metamorphic sole at an incipient plate contact, as is the case in other soles[15–17]. Other studies have reported zircon ages of 133–119 Ma for the same locality[48] and an adjacent one[32]. Apatite ages of 132–133 Ma have also been reported from the Bainang valley[48]. These authors interpreted some of the zircon and all apatite grains as igneous, implying that the older range of the 133–119 Ma dates would be protolith ages. However, the authors could not rule out a metamorphic origin. We note that the zircon ages overlap with 130–121 Ma Ar–Ar on hornblende cooling ages

for the same locality, as also reported from the well-studied Semail ophiolite-sole couple of Oman. Zircon of the Semail sole was demonstrated to have formed during the crystallization of partial melts generated during granulite metamorphism of the sole[15,53,54]. In addition, apatite is highly unstable in the presence of leucosome and will likely be consumed by melt producing reaction before crystallizing upon cooling[55]. The garnet Lu-Hf and hornblende Ar-Ar geochronology of the Bainang samples constrain prograde metamorphism near 144 Ma and cooling between 133 and 121 Ma; we therefore interpret the reported zircon and apatite ages from granulite of the XO metamorphic sole as dating the crystallization of a melt fraction following peak metamorphism, consistent with the leucosomes reported in the field and on samples[48]. Metamorphism of the XO sole involved a long prograde stage to granulite-facies peak metamorphism followed by rapid cooling from peak conditions, a similar scenario as reported for the Semail sole[15,56]. Definitive evidence for the age of the protolith in metamorphic soles remains elusive, or controversial at best, as reviewed elsewhere[13].

Our new data thus show that subduction of Neotethyan seafloor was underway by 144 Ma, providing the earliest direct evidence for northward subduction of Neo-Tethys seafloor south of the Lhasa Terrane. As the XO formed above this north-directed subduction directly at or close to the margin of the Lhasa Terrane[23,25,26,42], the underlying sole must have been buried following SI around the ocean-continent boundary (Fig. 3A, B). After nucleation of the subduction zone, the sole was transferred from the lower to the upper plate, accreting to Lhasa Terrane continental mantle (Fig. 3B, C).

Numerical models of this setting predicts that viscous necking of the subduction interface (Fig. 3D), trench retreat, and continental forearc hyperextension (Fig. 3E) followed as the increasing slab pull force eventually overcomes coupling at the subduction interface[27]. The sole was then exhumed between

**Table 1 Isotopic data.**

| Sample | Concentrations (ppm) | | Isotope data | | | | Lab | Lu-Hf age | 2 SD | $^{176}Hf/^{177}Hf_{initial}$ | 2 SD | MSWD |
|---|---|---|---|---|---|---|---|---|---|---|---|---|
| Analysis | Lu (ppm) | Hf (ppm) | $^{176}Lu/^{177}Hf$ | 2 SD | $^{176}Hf/^{177}Hf$ | 2 SD | | | | | | |
| BAIO1 | | | | | | | | | | | | |
| Grt-1 | 3.98 | 0.228 | 2.468 | 0.006 | 0.288472 | 0.000047 | UBC | - | - | - | - | - |
| Grt-2 | 4.55 | 0.299 | 2.155 | 0.005 | 0.287670 | 0.000061 | UBC | - | - | - | - | - |
| Grt-3 | 3.67 | 0.286 | 1.820 | 0.005 | 0.286808 | 0.000051 | UBC | - | - | - | - | - |
| Grt-4 | 4.09 | 0.264 | 2.190 | 0.005 | 0.287750 | 0.000014 | UBC | - | - | - | - | - |
| wr-1 | 0.607 | 1.87 | 0.04594 | 0.00011 | 0.281989 | 0.000021 | UBC | - | - | - | - | - |
| | - | - | - | - | - | - | - | 143.7 | 0.7 | 0.281868 | 0.000021 | 1.6 |
| CG64 | | | | | | | | | | | | |
| Grt-1 | 4.76 | 0.25 | 2.739 | 0.007 | 0.289393 | 0.000061 | UBC | - | - | - | - | - |
| Grt-2 | 5.50 | 0.37 | 2.134 | 0.005 | 0.287723 | 0.000058 | UBC | - | - | - | - | - |
| Grt-3 | 5.55 | 0.32 | 2.467 | 0.006 | 0.288650 | 0.000061 | UBC | - | - | - | - | - |
| Grt-4 | 5.73 | 0.36 | 2.264 | 0.006 | 0.288060 | 0.000063 | UBC | - | - | - | - | - |
| Wr-1 | 0.431 | 2.88 | 0.02124 | 0.00005 | 0.282027 | 0.000026 | UBC | - | - | - | - | - |
| | - | - | - | - | - | - | - | 144.6 | 0.9 | 0.281968 | 0.000026 | 0.52 |
| LUS17 | | | | | | | | | | | | |
| Grt-1 | 1.17 | 0.513 | 0.3228 | 0.0008 | 0.283980 | 0.000029 | UCSB | - | - | - | - | - |
| Grt-2 | 1.52 | 0.488 | 0.4427 | 0.0011 | 0.284302 | 0.000038 | UBC | - | - | - | - | - |
| Wr-1 | 0.358 | 1.81 | 0.02798 | 0.00007 | 0.283212 | 0.000019 | UCSB | - | - | - | - | - |
| | - | - | - | - | - | - | - | 140.1 | 4.5 | 0.283138 | 0.000020 | 0.12 |
| LUS12 | | | | | | | | | | | | |
| Grt-1 | 1.29 | 0.360 | 0.5062 | 0.0013 | 0.284401 | 0.000031 | UCSB | - | - | - | - | - |
| Grt-2 | 1.01 | 0.333 | 0.4308 | 0.0011 | 0.284211 | 0.000039 | UBC | - | - | - | - | - |
| Grt-3 | 1.28 | 0.482 | 0.3771 | 0.0009 | 0.284047 | 0.000031 | UBC | - | - | - | - | - |
| Grt-4[a] | 1.57 | 0.419 | 0.5322 | 0.0013 | 0.284579 | 0.000017 | UCSB | - | - | - | - | - |
| Wr-1 | 0.435 | 1.92 | 0.03207 | 0.00008 | 0.283124 | 0.000019 | UCSB | - | - | - | - | - |
| | - | - | - | - | - | - | - | 144.3 | 3.5 | 0.283037 | 0.000020 | 0.29 |

Lu-Hf geochronology.
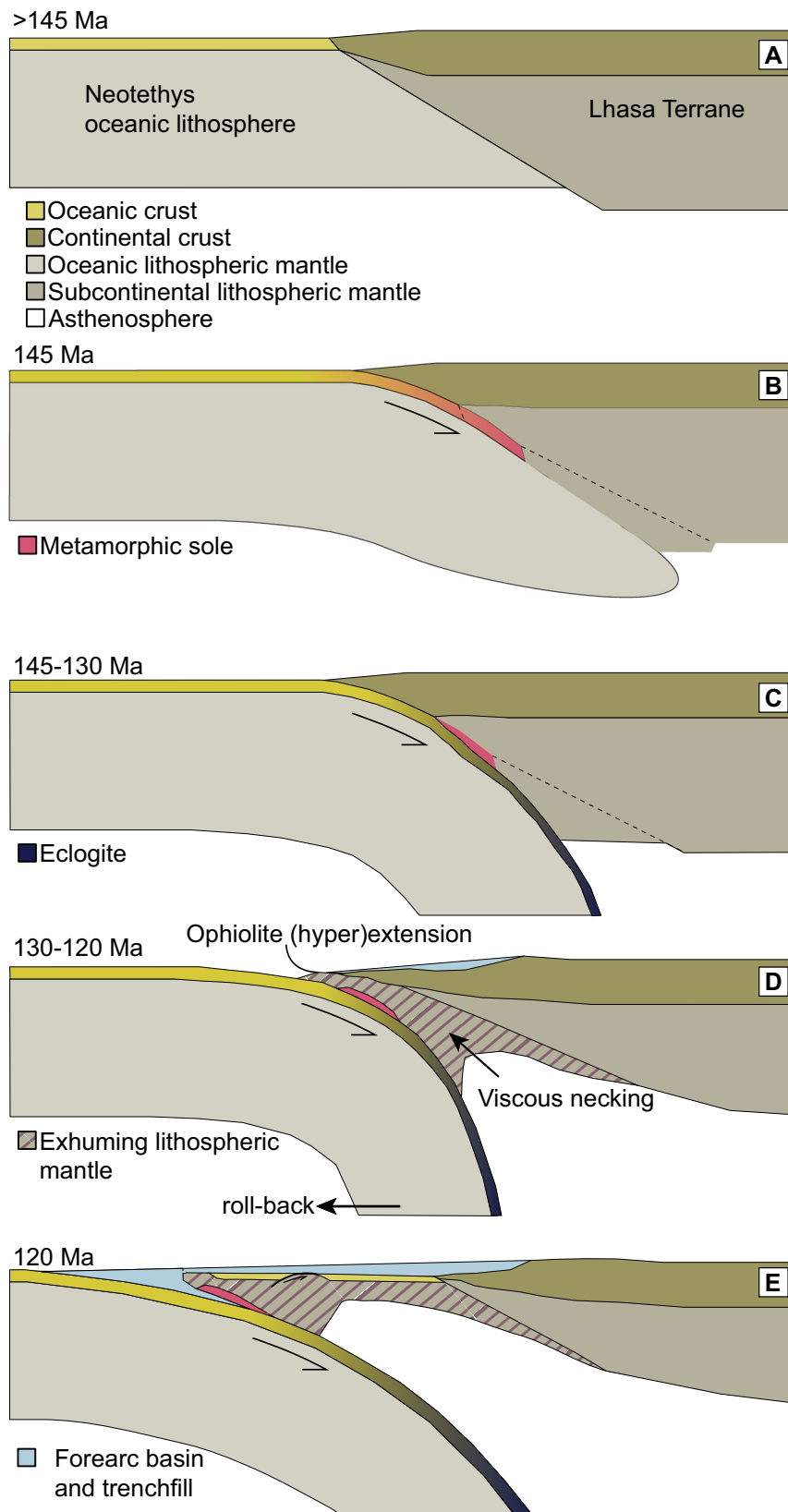[a]Coarse pieces retrieved from 1st stage crushing (>800 μm); all other garnet was <100 μm size.

**Fig. 3 Tectonic model for sole formation during subduction initiation under a continental margin. A** lithospheric cross-section of the pre-subduction Tibetan margin, (**B**) forced subduction initiation at the continental margin causes metamorphism in the lower plate and garnet growth, (**C**) increasing slab pull force during convergence causes slab roll-back, (**D**) slab-pull force reaches a critical point triggering viscous necking of the subduction interface, trench retreat, upper plate extension, and exhumation of the metamorphic sole. (**E**) Continued northward subduction of Neotethyan oceanic lithosphere under the Lhasa Terrane margin with the Xigaze ophiolite and sole forming the basement of the clastic forearc basin.

130 and 120 Ma, as indicated by sole cooling ages, synchronous with limited mantle melting and generation of the XO crust. The forearc extension model[3,11,26,27] following induced subduction initiation therefore provides a comprehensive explanation for the lag time between burial and exhumation of soles as well as a mechanism for sole exhumation synchronous with upper plate extension and supra-subduction zone ophiolite spreading. Ensuing north-directed subduction of Neotethyan oceanic lithosphere resulted in the formation of the Gangdese magmatic arc at the southern margin of the Lhasa Terrane[34] and deposition of the Xigaze basin clastic sediments on the XO[24], until obduction over the Tethyan Himalayan continental margin[30,47].

**Soles and subduction initiation at continental margins.** Our new results demonstrate that garnet growth in the Tibetan sole was already underway 14 Ma before forearc extension and formation of the Xigaze Ophiolite. This has several first-order implications for the regional tectonic evolution, and for the formation of soles in general.

First, northward underthrusting of oceanic lithosphere below the Lhasa block largely predating ophiolite formation implies that SI was induced by far-field stresses[15], ruling out spontaneous subduction initiation. The 14 Ma lag time between lower plate burial (Lu-Hf garnet ages of the sole) and upper plate extension (U-Pb zircon ages of ophiolitic crust) and associated, synchronous, rapid sole exhumation and cooling (U-Pb zircon and apatite and Ar-Ar hornblende ages of the sole) is longer than in Oman (8 Ma[15]), California (~10 Ma[16]), and Turkey (~12 Ma[17,57]). This longer delay in Tibet may possibly reflect a stronger coupling at the subduction interface, consistent with a thicker continental upper plate and thus a longer plate interface. However, some of the timing estimates could also be minimum estimates. Still, the similarity and differences in timing is an important point and an avenue of future research that needs to be explored.

Second, the trigger of SI should be sought at or before 144 Ma. The identification of this trigger is beyond the scope of this paper, but we note that SI occurred as the Lhasa Terrane was approaching the Eurasian margin[58], if not colliding with it[35]. Subduction may thus have been initiated by transference, perhaps diachronously: the forces required to induce SI at a continental margin are significantly lowered in the case of lateral propagation along inherited rift structures[59].

Third, the 144 Ma garnet growth age for the Xigaze ophiolite sole directly demonstrates that soles also form during subduction below continental lithosphere, as proposed before[19] arguing against the inference that ophiolite-sole couples are diagnostic of intra-oceanic SI. Moreover, the P-T conditions, lithologies, mineralogy, and chemistry of the XO sole rocks are typical of soles worldwide, including those that unequivocally formed in intra-oceanic settings (e.g., in the Mirdita Ophiolite[60]). This is surprising, as peak temperatures in excess of 850 °C in soles have long been inferred to be indicative of subduction initiation under a hot mantle hanging wall[3,5,8,9]. Here, we demonstrate that SI under a continental mantle resulted in a metamorphic sole that recorded the same P-T conditions[22,32]. Perhaps this demonstrates that the mantle below the southern Lhasa margin was anomalously hot, e.g. related to the arc magmatism that affected this region already since Jurassic times or before[30,34]. On the other hand, metamorphic soles of Oman and Turkey formed by subduction initiation in ancient lithosphere, devoid of pre-existing magmatism that could have caused elevated temperatures[18,19], and these soles recorded near-identical conditions as the XO sole[7,15,17,61]. So regardless of dynamic interpretations and speculations on the causes of these high-temperature conditions, our analysis shows that the metamorphic conditions recorded are the same for soles that form by SI near a mid-ocean ridge[62–64], along ancient transform faults in >100 Ma old oceanic lithosphere[18,19], or even along a continental margin as we show here, spanning a remarkable variety of settings with contrasting thermal gradients. Moreover, these conditions are consistently found for soles that date back at least 480 Ma[8,65]. We thus conclude that the sole formation process is irrespective of the setting of SI but may rather relate to the subduction initiation process and/or the formation of the overlying ophiolite during forearc extension, processes implicitly common to all soles. Constraints from metamorphic soles may accordingly be considered generic and provide key insight in the processes that governed the initiation of Phanerozoic subduction zones in general, regardless of the setting in which they formed.

## Methods

Samples were collected from four adjacent outcrops (see Fig. 1D) around location CG-64 at a longitude of 89.33311°E and a latitude of 29.14045°N. Thin sections were mapped using a μ-X-ray fluorescence spectroscopy (μ-XRF) Tornado M4 instrument at Université Laval. Analytical conditions were a 20 μm step size with an acquisition time of 3 ms per pixel. The X-ray tube was set at 50 keV and 300 mA for a total acquisition time of c. 2.5 h per sample. Garnet grains showing the strongest major element zoning from core to rim, mainly observed as a bell-shaped spessartine zoning, were selected for LA-ICP-MS Lutetium mapping.

Trace element analyses of garnet were performed by LA-ICP-MS at LabMaTer (Université du Québec à Chicoutimi), using a Australian Scientific Instruments RESOlution 193 nm excimer laser and an S155 Laurin Technic ablation cell system coupled to an Agilent 7900 quadrupole ICP-MS. High-resolution mapping was performed in-situ on garnet to document trace element zoning. Analytical conditions were a 20 μm beam moving at a speed of 80 μm s$^{-1}$ and pulsing of 30 Hz at 5 J cm$^{-2}$ in a 4 ms per mass cycle. The synthetic reference glass GSE-1G[66] was used for calibration. Data reduction was processed with the Iolite freeware[67] using mean EPMA $^{29}$Si data as an internal standard.

Lutetium-hafnium chronology was performed in two separate laboratories. Samples were crushed and garnet fractions were hand-picked under a binocular microscope and contained all sizes of grain and random core/rim proportions. Garnet and whole rock (WR) splits from samples LUS12 and LUS17 were analyzed at the Department of Earth Sciences, University of California, Santa Barbara. Additional garnet materials from these samples, as well as all analyses for samples BAI01 and CG64 were done at the Pacific Centre for Isotopic and Geochemical Research, University of British Columbia, Vancouver. Both methods utilize mixed $^{176}$Lu-$^{180}$Hf isotope tracers made from different base metals and oxides, and independently developed and calibrated[68,69]. For Lu-Hf analysis, garnet fractions and WR powder were transferred to screw-top PFA vials. Garnet grains were washed using de-ionized water and ethanol, dried, transferred to PFA vials, and bathed in 1 N HCl at room temperature for 1 h. After removing the HCl, samples were mixed with a $^{176}$Lu-$^{180}$Hf isotope tracer with matrix-equivalent Lu/Hf ratio, and digested through repeated addition of HF:HNO$_3$:HClO$_4$ and 6 N HCl, each step followed by evaporation to dryness. After tracer admixing, the WR powders were digested in stainless-steel Parr vessels at 180 °C for 7 days using HF:HNO$_3$. After digestion, all samples were dried, re-dissolved in 6 N HCl, diluted to 3 N HCl using de-ionized H$_2$O, and centrifuged. The solution containing the garnet elemental solute was then loaded onto polypropylene columns containing a 1-ml Ln-Spec resin bed before being analyzed through REE-HFSE chromatography[70].

Hafnium and Lutetium isotope analyses were done with a Nu Instruments *Plasma*/multi-collector inductively coupled plasma mass spectrometry (MC-ICPMS) instrument. For Lu analyses, isobaric interference of $^{176}$Yb on $^{176}$Lu was corrected using an exponential correlation of $^{176}$Yb/$^{171}$Yb and $^{174}$Yb/$^{171}$Yb, calibrated through replicate analyses of NIST Yb solution standards at different concentrations 10-100 ppb[71]; For Hf isotope analyses, $^{180}$Ta and $^{180}$W interferences were corrected by analyzing $^{181}$Ta and $^{183}$W. Mass bias was assumed to follow an exponential law and was corrected applying $^{179}$Hf/$^{177}$Hf = 0.7325 and $^{173}$Yb/$^{171}$Yb = 1.1296[72]. Drift was corrected by assuming linear time dependence. Hafnium isotope values are reported relative to those of ATI-475, an in-house-developed Hf isotope reference material made from the original Hf metal ingots from which the international reference solution JMC-475 was made, with $^{176}$Hf/$^{177}$Hf = 0.28216[73]. Replicate analyses of ATI-475 done at concentrations bracketing that of samples helped estimate external reproducibility of $^{176}$Hf/$^{177}$Hf and was 38 ppm during the course of our analytical session[74]. The Lu-Hf isochrons were established using a $\lambda^{176}$Lu decay constant of $1.867 \times 10^{-11}$ yr$^{-1}$[75,76]. All uncertainties are cited at the 2-s.d. level.

## Data availability

## References

1. Stern, R. J. Subduction initiation: spontaneous and induced. *Earth Planet. Sci. Lett.* **226**, 275–292 (2004).
2. Stern, R. J. & Gerya, T. Subduction initiation in nature and models: a review. *Tectonophysics* **746**, 173–198 (2018).
3. Wakabayashi, J. & Dilek, Y. Spatial and temporal relationships between ophiolites and their soles; a test of models of forearc ophiolite genesis. *Geol. Soc. Am. Spec. Pap.* 349, 53–64 (2000).
4. Williams, H. & Smyth, W. R. Metamorphic aureoles beneath ophiolite suites and alpine peridotites; tectonic implications with west Newfoundland examples. *Am. J. Sci.* **273**, 594–621 (1973).
5. Spray, J. G. Possible causes and consequences of upper mantle decoupling and ophiolite displacement. *Geol. Soc. Lond. Special Publ.* **13**, 255–268 (1984).
6. Jamieson, R. A. P-T paths from high temperature shear zones beneath ophiolites. *J. Metamorph. Geol.* **4**, 3–22 (1986).
7. Agard, P. et al. Plate interface rheological switches during subduction infancy: Control on slab penetration and metamorphic sole formation. *Earth Planet. Sci. Lett.* **451**, 208–220 (2016).
8. Jamieson, R. A. Formation of rnetamorphic aureoles beneath ophiolites—Evidence from the St. Anthony Complex, Newfoundland. *Geology* https://doi.org/10.1130/0091-7613 (1980).
9. Hacker, B. R. Simulation of the metamorphic and deformational history of the metamorphic sole of the Oman Ophiolite. *J. Geophys. Res.* https://doi.org/10.1029/JB095iB04p04895 (1990).
10. Stern, R. J., Reagan, M., Ishizuka, O., Ohara, Y. & Whattam, S. To understand subduction initiation, study forearc crust: To understand forearc crust, study ophiolites. *Lithosphere* **4**, 469–483 (2012).
11. Bloomer, S. H. et al. Early arc volcanism and the ophiolitic problem: a perspective from drilling in the western Pacific. *Active Margins And Marginal Basins Of The Western Pacific, AGU Geophysical Monograph Series,* 88, 1–30 (1995).
12. van Hinsbergen, D. J. J. et al. Dynamics of intraoceanic subduction initiation: 2. Suprasubduction zone ophiolite formation and metamorphic sole exhumation in context of absolute plate motions. *Geochem. Geophys. Geosyst.* **16**, 1771–1785 (2015).
13. Wakabayashi, J. & Shimabukuro, D. H. The contrasting geologic record of inferred "hot" intraoceanic and "cold" continental margin subduction initiation in *Geol. Soc. Am. Spec. Pap.* 557, 169–194 (2022).
14. Hacker, B., Mosenfelder, J. & Gnos, E. Rapid emplacement of the Oman ophiolite: Thermal and geochronologic constraints. *Tectonics* **15**, 1230–1247 (1996).
15. Guilmette, C. et al. Forced subduction initiation recorded in the sole and crust of the Semail Ophiolite of Oman. *Nat. Geosci.* **11**, 688–695 (2018).
16. Mulcahy, S. R., Starnes, J. K., Day, H. W., Coble, M. A. & Vervoort, J. D. Early onset of Franciscan subduction. *Tectonics* **37**, 1194–1209 (2018).
17. Pourteau, A. et al. Thermal evolution of an ancient subduction interface revealed by Lu–Hf garnet geochronology, Halilbağı Complex (Anatolia). *Geosci. Front.* **10**, 127–148 (2019).
18. van Hinsbergen, D. J. J. et al. A record of plume-induced plate rotation triggering seafloor spreading and subduction initiation. *Nat. Geosci.* **14**, 626–630 (2021).
19. van Hinsbergen, D. J., Maffione, M., Koornneef, L. M. & Guilmette, C. Kinematic and paleomagnetic restoration of the Semail ophiolite (Oman) reveals subduction initiation along an ancient Neotethyan fracture zone. *Earth Planet. Sci. Lett.* **518**, 183–196 (2019).
20. Hébert, R. et al. The Indus–Yarlung Zangbo ophiolites from Nanga Parbat to Namche Barwa syntaxes, southern Tibet: First synthesis of petrology, geochemistry, and geochronology with incidences on geodynamic reconstructions of Neo-Tethys. *Gondwana Res.* **22**, 377–397 (2012).
21. Guilmette, C., Hébert, R., Wang, C. & Villeneuve, M. Geochemistry and geochronology of the metamorphic sole underlying the Xigaze Ophiolite, Yarlung Zangbo Suture Zone, South Tibet. *Lithos* **112**, 149–162 (2009).
22. Guilmette, C., Hébert, R., Dupuis, C., Wang, C. & Li, Z. Metamorphic history and geodynamic significance of high-grade metabasites from the ophiolitic mélange beneath the Yarlung Zangbo ophiolites, Xigaze area, Tibet. *J. Asian Earth Sci.* **32**, 423–437 (2008).
23. Huang, W. et al. Lower Cretaceous Xigaze ophiolites formed in the Gangdese forearc: Evidence from paleomagnetism, sediment provenance, and stratigraphy. *Earth Planet. Sci. Lett.* **415**, 142–153 (2015).
24. Wang, J.-G., Hu, X., Garzanti, E., An, W. & Liu, X.-C. The birth of the Xigaze forearc basin in southern Tibet. *Earth Planet. Sci. Lett.* **465**, 38–47 (2017).
25. Li, Y. et al. Detachment faulting in the Xigaze ophiolite southern Tibet: New constraints on its origin and implications. *Gondwana Res.* **94**, 44–55 (2021).
26. Maffione, M. et al. Forearc hyperextension dismembered the south Tibetan ophiolites. *Geology* **43**, 475–478 (2015).
27. Butler, J. P. & Beaumont, C. Subduction zone decoupling/retreat modeling explains south Tibet (Xigaze) and other supra-subduction zone ophiolites and their UHP mineral phases. *Earth Planet. Sci. Lett.* **463**, 101–117 (2017).
28. Nicolas, A. et al. The Xigaze ophiolite (Tibet): a peculiar oceanic lithosphere. *Nature* **294**, 414–417 (1981).
29. Liu, T. et al. The Xigaze ophiolite: fossil ultraslow-spreading ocean lithosphere in the Tibetan Plateau. *J. Geol. Soc.* https://doi.org/10.1144/jgs2020-208 (2021).
30. Kapp, P. & DeCelles, P. G. Mesozoic–Cenozoic geological evolution of the Himalayan-Tibetan orogen and working tectonic hypotheses. *Am. J. Sci.* **319**, 159–254 (2019).
31. Hu, H. & Stern, R. J. Early Cretaceous subduction initiation beneath southern Tibet caused the northward flight of India. *Geosci. Front.* **11**, 1123–1131 (2020).
32. Zhang, C. et al. Subduction re-initiation at dying ridge of Neo-Tethys: Insights from mafic and metamafic rocks in Lhaze ophiolitic mélange, Yarlung-Tsangbo Suture Zone. *Earth Planet. Sci. Lett.* https://doi.org/10.1016/j.epsl.2019.07.009 (2019).
33. Liu, W. et al. The Late Jurassic Zedong ophiolite: a remnant of subduction initiation within the Yarlung Zangbo Suture Zone (southern Tibet) and its tectonic implications. *Gondwana Res.* **78**, 172–188 (2020).
34. Zhu, D.-C. et al. The Lhasa Terrane: Record of a microcontinent and its histories of drift and growth. *Earth Planet. Sci. Lett.* **301**, 241–255 (2011).
35. Li, S., Yin, C., Guilmette, C., Ding, L. & Zhang, J. Birth and demise of the Bangong-Nujiang Tethyan Ocean: a review from the Gerze area of central Tibet. *Earth-Sci. Rev.* **198**, 102907 (2019).
36. Zhang, L.-L., Liu, C.-Z., Wu, F.-Y., Ji, W.-Q. & Wang, J.-G. Zedong terrane revisited: an intra-oceanic arc within Neo-Tethys or a part of the Asian active continental margin? *J. Asian Earth Sci.* **80**, 34–55 (2014).
37. Dubois-Côté, V. et al. Petrological and geochemical evidence for the origin of the Yarlung Zangbo ophiolites, southern Tibet. *Chem. Geol.* **214**, 265–286 (2005).
38. Ziabrev, S. et al. Precise radiolarian age constraints on the timing of ophiolite generation and sedimentation in the Dazhuqu terrane, Yarlung–Tsangpo suture zone, Tibet. *J. Geol. Soc.* **160**, 591–599 (2003).
39. Chan, G. H. N. et al. U–Pb zircon ages for Yarlung Tsangpo suture zone ophiolites, southwestern Tibet and their tectonic implications. *Gondwana Res.* **27**, 719–732 (2015).
40. Xu, Y. et al. The complex life cycle of oceanic lithosphere: A study of Yarlung-Zangbo ophiolitic peridotites, Tibet. *Geochim. Cosmochim. Acta* **277**, 175–191 (2020).

41. Göpel, C., Allègre, C. J. & Xu, R.-H. Lead isotopic study of the Xigaze ophiolite (Tibet): the problem of the relationship between magmatites (gabbros, dolerites, lavas) and tectonites (harzburgites). *Earth Planet. Sci. Lett.* **69**, 301–310 (1984).

42. Gong, X.-H. et al. Recycling of ancient subduction-modified mantle domains in the Purang ophiolite (southwestern Tibet). *Lithos* **262**, 11–26 (2016).

43. Guilmette, C. et al. Discovery of a dismembered metamorphic sole in the Saga ophiolitic mélange, South Tibet: assessing an Early Cretaceous disruption of the Neo-Tethyan supra-subduction zone and consequences on basin closing. *Gondwana Res.* **22**, 398–414 (2012).

44. Dupuis, C. et al. The Yarlung Zangbo Suture Zone ophiolitic mélange (southern Tibet): new insights from geochemistry of ultramafic rocks. *J. Asian Earth Sci.* **25**, 937–960 (2005).

45. Dupuis, C. et al. Petrology and geochemistry of mafic rocks from mélange and flysch units adjacent to the Yarlung Zangbo Suture Zone, southern Tibet. *Chem. Geol.* **214**, 287–308 (2005).

46. Ziabrev, S. V., Aitchison, J. C., Abrajevitch, A. V., Davis, A. M. & Luo, H. Bainang Terrane, Yarlung–Tsangpo suture, southern Tibet (Xizang, China): a record of intra-Neotethyan subduction–accretion processes preserved on the roof of the world. *J. Geol. Soc.* **161**, 523–539 (2004).

47. Ding, L., Kapp, P. & Wan, X. Paleocene-Eocene record of ophiolite obduction and initial India-Asia collision, south central Tibet. *Tectonics* **24**, n/a–n/a (2005).

48. Duan, W.-Y., Li, X.-P., Schertl, H.-P., Willner, A. P. & Sun, G.-M. "Hot" subduction initiation and the origin of the Yarlung-Tsangbo ophiolites, southern Tibet: New insights from ultrahigh temperature metamorphic soles. *Earth Planet. Sci. Lett.* **591** https://doi.org/10.1016/j.epsl.2022.117610 (2022).

49. Wang, B.-D. et al. Evolution of the Bangong–Nujiang Tethyan ocean: Insights from the geochronology and geochemistry of mafic rocks within ophiolites. *Lithos* **245**, 18–33 (2016).

50. Scherer, E. E., Cameron, K. L. & Blichert-Toft, J. Lu–Hf garnet geochronology: closure temperature relative to the Sm–Nd system and the effects of trace mineral inclusions. *Geochim. Cosmochim. Acta* **64**, 3413–3432 (2000).

51. Smit, M. A., Scherer, E. E. & Mezger, K. Lu–Hf and Sm–Nd garnet geochronology: chronometric closure and implications for dating petrological processes. *Earth Planet. Sci. Lett.* **381**, 222–233 (2013).

52. Bloch, E., Ganguly, J., Hervig, R. & Cheng, W. 176 Lu–176 Hf geochronology of garnet I: experimental determination of the diffusion kinetics of Lu 3+ and Hf 4+ in garnet, closure temperatures and geochronological implications. *Contrib. Mineral. Petrol.* **169**, 12 (2015).

53. Rioux, M. et al. Synchronous formation of the metamorphic sole and igneous crust of the Semail ophiolite: New constraints on the tectonic evolution during ophiolite formation from high-precision U–Pb zircon geochronology. *Earth Planet. Sci. Lett.* **451**, 185–195 (2016).

54. Warren, C. J., Parrish, R. R., Waters, D. J. & Searle, M. P. Dating the geologic history of Oman's Semail ophiolite: insights from U-Pb geochronology. *Contrib. Mineral. Petrol.* **150**, 403–422 (2005).

55. O'Sullivan, G., Chew, D., Kenny, G., Henrichs, I. & Mulligan, D. The trace element composition of apatite and its application to detrital provenance studies. *Earth-Sci. Rev.* https://doi.org/10.1016/j.earscirev.2019.103044 (2020).

56. Soret, M. et al. Timescales of subduction initiation and evolution of subduction thermal regimes. *Earth Planet. Sci. Lett.* https://doi.org/10.1016/j.epsl.2022.117521 (2022).

57. Pourteau, A., Oberhänsli, R., Candan, O., Barrier, E. & Vrielynck, B. Neotethyan closure history of western Anatolia: a geodynamic discussion. *Int. J. Earth Sci.* **105**, 203–224 (2016).

58. Li, Z. et al. Paleomagnetic constraints on the Mesozoic drift of the Lhasa terrane (Tibet) from Gondwana to Eurasia. *Geology* **44**, 727–730 (2016).

59. Zhou, X., Li, Z.-H., Gerya, T. V. & Stern, R. J. Lateral propagation–induced subduction initiation at passive continental margins controlled by preexisting lithospheric weakness. *Sci. Adv.* **6**, eaaz1048 (2020).

60. Maffione, M. et al. Dynamics of intraoceanic subduction initiation: 1. Oceanic detachment fault inversion and the formation of supra-subduction zone ophiolites. *Geochem. Geophys. Geosyst.* **16**, 1753–1770 (2015).

61. Soret, M., Agard, P., Dubacq, B., Plunder, A. & Yamato, P. Petrological evidence for stepwise accretion of metamorphic soles during subduction infancy (Semail ophiolite, Oman and UAE). *J. Metamorph. Geol.* **35**, 1051–1080 (2017).

62. Liati, A., Gebauer, D. & Fanning, C. M. The age of ophiolitic rocks of the Hellenides (Vourinos, Pindos, Crete): first U–Pb ion microprobe (SHRIMP) zircon ages. *Chem. Geol.* **207**, 171–188 (2004).

63. Maffione, M. & van Hinsbergen, D. J. J. Reconstructing plate boundaries in the Jurassic Neo-Tethys from the East and West Vardar Ophiolites (Greece, Serbia). *Tectonics* https://doi.org/10.1002/2017tc004790 (2018).

64. Myhill, R. Constraint on the evolution of the Mesohellenic Ophiolites in *Geol. Soc. Am. Spec. Pap.* **480**, 75 (2011).

65. Dewey, J. F. & Casey, J. F. The sole of an ophiolite: the Ordovician Bay of Islands Complex, Newfoundland. *J. Geol. Soc.* **170**, 715–722 (2013).

66. Jochum, K. P., Willbold, M., Raczek, I., Stoll, B. & Herwig, K. Chemical Characterisation of the USGS Reference Glasses GSA-1G, GSC-1G, GSD-1G, GSE-1G, BCR-2G, BHVO-2G and BIR-1G Using EPMA, ID-TIMS, ID-ICP-MS and LA-ICP-MS. *Geostand. Geoanal. Res.* **29**, 285–302 (2005).

67. Paton, C., Hellstrom, J., Paul, B., Woodhead, J. & Hergt, J. Iolite: Freeware for the visualisation and processing of mass spectrometric data. *J. Anal. At. Spectrom.* **26**, 2508–2518 (2011).

68. Smit, M. A., Hacker, B. R. & Lee, J. Tibetan garnet records early Eocene initiation of thickening in the Himalaya. *Geology* **42**, 591–594 (2014).

69. Cutts, J. & Smit, M. Rates of Deep Continental Burial From Lu-Hf Garnet Chronology and Zr-in-Rutile Thermometry on (Ultra) high-Pressure Rocks. *Tectonics* **37**, 71–88 (2018).

70. Münker, C., Weyer, S., Scherer, E. & Mezger, K. Separation of high field strength elements (Nb, Ta, Zr, Hf) and Lu from rock samples for MC-ICPMS measurements. *Geochem. Geophys. Geosyst.* **2**, 1064 (2001).

71. Blichert-Toft, J., Boyet, M., Télouk, P. & Albarède, F. 147Sm–143Nd and 176Lu–176Hf in eucrites and the differentiation of the HED parent body. *Earth Planet. Sci. Lett.* **204**, 167–181 (2002).

72. Vervoort, J. D., Patchett, P. J., Söderlund, U. & Baker, M. Isotopic composition of Yb and the determination of Lu concentrations and Lu/Hf ratios by isotope dilution using MC-ICPMS. *Geochem. Geophys. Geosyst.* **5**, n/a–n/a (2004).

73. Vervoort, J. D. & Blichert-Toft, J. Evolution of the depleted mantle: Hf isotope evidence from juvenile rocks through time. *Geochim. Cosmochim. Acta* **63**, 533–556 (1999).

74. Bizzarro, M., Baker, J. A. & Ulfbeck, D. A new digestion and chemical separation technique for rapid and highly reproducible determination of Lu/Hf and Hf isotope ratios in geological materials by MC-ICP-MS. *Geostand. Newslett.* **27**, 133–145 (2003).

75. Söderlund, U., Patchett, P. J., Vervoort, J. D. & Isachsen, C. E. The 176Lu decay constant determined by Lu–Hf and U–Pb isotope systematics of Precambrian mafic intrusions. *Earth Planet. Sci. Lett.* **219**, 311–324 (2004).

76. Scherer, E., Münker, C. & Mezger, K. Calibration of the lutetium-hafnium clock. *Science* **293**, 683–687 (2001).

77. Wang, X. B., Xiao, X. C., Cao, Y. G. & Zheng, H. X. Geological map of the ophiolite zone along the middle Yarlung Zangbo River (Tsangpo River), Xizang (Tibet): Beijing, China,. (Academy of Geological Sciences, 1984).

## Acknowledgements

## Author contributions

C.G. designed the project, led field work, interpreted the data, and wrote the manuscript. D.v.H. participated in field work, interpreted the data, and helped write the manuscript. M.S. conducted isotopic analysis, interpreted the data, and helped write the manuscript. A.G. conducted trace element mapping, reduced the data, and helped write the manuscript. F.F.R. helped interpret the data, prepared figures, and helped write the manuscript. J.P.B. participated in field work, contributed samples, and helped interpret the data. M.M. participated in field work and helped interpret the data. S.L. organized and participated in field work and helped interpret the data. K.H. participated in field work and helped interpret the data and edit the manuscript.

## Competing interests

The authors declare no competing interests.

## Additional information